Ab Initio Direct Dynamics Study of OOH + H → H_2 + $^3O_2$†

Glenn M. Thurman and Rozeanne Steckler*

Department of Chemistry, San Diego State University and San Diego Supercomputer Center, P.O. Box 85608, San Diego, California 92186-9784

Received: April 26, 2000; In Final Form: September 26, 2000

We report the first-principles computation of rate constants for the atmospheric reaction OOH + H → H_2 + $^3O_2$, by combining variational transition state theory (VTST) and high-level electronic structure theory. Using the direct dynamics approach, the rate constants were computed, directly, using ab initio electronic structure theory at the second-order many-body perturbation theory (MBPT(2)) and coupled-cluster singles-and-doubles with a perturbative triples correction (CCSD(T)) levels, and variational transition state theory including tunneling. The computed room-temperature rate constant, 6.85×10^{-12} cm^3 molecule^{-1} s^{-1}, is in excellent agreement with experiment (6.96×10^{-12}). However, we do not find that the rate constant is nearly constant over the temperature range $250 \leq T \leq 300$ K as suggested by experiment. In addition, the calculations suggest the reaction is non-Arrhenius over both the temperature ranges 150−400 K and 150−800 K. The computed temperature dependence of the rate constant is well represented by the three-parameter fit: $k = (6.99 \times 10^{-15})\ T^{1.10} \exp(187/T)$.

I. Introduction

An understanding of ozone chemistry above the stratopause is of great importance to the problem of ozone depletion in the stratosphere. The upper stratosphere and mesosphere contain less than 25% of the total atmospheric ozone yet constitute the photochemical source region for ozone in the lower stratosphere. High altitude ozone chemistry is controlled by some of the same catalytic cycles that are important in the lower stratosphere, but the chemistry at high altitude is simpler because a smaller number of reactions are involved. It is therefore possible to test some important parts of stratospheric models under the simplified conditions of the upper atmosphere.

The only important source of "odd" oxygen (O and O_3, in contrast to the "even" O_2) above 30 km is the photolysis of molecular oxygen. The most significant sinks for odd oxygen in the mesosphere are the reactions of atomic oxygen with the HO_X family:

$$O + HO \rightarrow H + O_2 \quad \text{(R1)}$$

$$O + HO_2 \rightarrow HO + O_2 \quad \text{(R2)}$$

Production of HO_X below 60 km is dominated by

$$O(^1D) + H_2O \rightarrow HO + HO \quad \text{(R3)}$$

which competes with HO_X loss by

$$HO + HO_2 \rightarrow H_2O + O_2 \quad \text{(R4)}$$

Reaction (R4) accounts for over 90% of the HO_X loss below 70 km. Above 65 km, HO_X is produced mainly by

$$H_2O + h\nu \rightarrow H + HO \quad \text{(R5)}$$

Above 70 km, the main removal reactions for HO_X are two of three possible pathways of

$$H + HO_2 \rightarrow \text{products} \quad \text{(R6)}$$

i.e., reactions (R6b) and (R6c)

$$H + HO_2 \rightarrow HO + HO \quad \text{(R6a)}$$

$$\rightarrow H_2O + O \quad \text{(R6b)}$$

$$\rightarrow H_2 + {}^3O_2 \quad \text{(R6c)}$$

The greatest HO_X loss is through reaction (R6c). Reaction (R6a) has the larger rate constant, but HO_X is regenerated as HO.

Recent mesospheric model results show that calculated ozone concentrations near the extremely cold mesopause (80 km, 190 K) are very sensitive to the magnitude of the rate constant of reaction (R6c). This is due to the importance of reaction (R6c) to the HO_X budget in that region. The rate constant for reaction (R6c) is highly uncertain. Moreover, it has been measured only at or near room temperature, hence its temperature dependence is also very poorly determined. Low-temperature rate constants for reaction (R6c) are crucial to models of the mesosphere, as indicated earlier.

The overall rate constant and/or branching ratios for reaction (R6) have been determined experimentally in a large number of studies since 1963.[1−11] Near 300 K, values of the overall rate constant k_{R6} range from 4.6×10^{-11} to 8.7×10^{-11} cm^3 molecule^{-1} sec^{-1}, a factor of 2 in uncertainty. Wide ranging differences in the branching ratio, k_{R6c}/k_{R6}, have also been found: reported values range from 0.09 to 0.62 near 300 K. To obtain k_{R6c}, both the overall rate constant, k_{R6}, and branching ratio, k_{R6c}/k_{R6}, must be determined. But k_{R6} and k_{R6c}/k_{R6} have been determined together in only three studies, Hack et al.,[7] Sridharan et al.,[10] and Keyser,[11] yielding only three values of k_{R6c}, all at room temperature. These values run from 1.66×10^{-11} to 6.96×10^{-11} cm^3 molecule^{-1} s^{-1}. The two most recent

† Part of the special issue "Aron Kuppermann Festschrift".

10.1021/jp001599s CCC: $20.00
Published on Web 11/08/2000

studies, Sridharan et al.[10] and Keyser,[11] obtain direct kinetic data, and the rate constant determinations are in very good agreement.

The discordance in rates and branching ratios in the earlier studies can be attributed in part to the indirect methods used in those studies. Some of their results were based on ratios of k_{R6} to other rate constants whose values have since been revised. Uncertainty in their assumptions regarding complicated reaction schemes also contributes to the uncertainty in the rate constants.

Accurate rate constants for atmospheric reactions are needed for modeling ozone depletion. These have been difficult to obtain experimentally for reasons discussed above. Moreover, rate constants are often needed over a wider range of temperature than is obtainable in practice. This is the case for H + HO_2 where there are no experimental studies on the temperature dependence of k_{R6c}. Advances in high-performance computing have made practical ab initio calculation of rate constants for atmospheric reactions to within experimental accuracy. This paper reports the application of *direct dynamics*, the integration of electronic structure and dynamics calculations, to the calculation of the ab initio rate constant for reaction (R6c) over a wide range of the temperatures. The room-temperature rate constant is compared with the experimental values obtained by Sridharan et al.,[10] and Keyser.[11] The temperature dependence of the rate constant and the implications for atmospheric chemistry are discussed.

II. Methods

A. Dynamics. The canonical form of variational transition state theory,[12−15] called canonical variational theory (CVT), was used for the dynamics calculations. Tunneling corrections are computed using the centrifugal-dominant semiclassical ground state (CD-SCSAG).[16] In accordance with the direct dynamics[17−19] method, a global potential energy surface (PES) was not used in these calculations. Instead, electronic structure calculations served as the pseudo-PES, providing, as the minimum energy path (MEP) was calculated, the PES information required for following the MEP and for the rate constant calculation, which includes geometries, first derivatives, and frequencies.

For ab initio rate constants to be of value to atmospheric modeling, they must be calculated to within experimental accuracy. Obtaining for the rate constant calculation PES information that is both complete and accurate enough to meet this standard requires electronic structure computations with large basis sets and a level of theory that recovers a large fraction of the correlation energy. Hence, calculating the partition function of each generalized transition state along the reaction path represents a heavy computational cost per point. At 2000 points per reaction path (a typical number), it is clear that at a level of theory high enough (e.g., CCSD(T)) to yield the accurate rate constants we seek, even direct dynamics is too expensive.

An outstanding compromise between cost and accuracy may be achieved with the new interpolation method called interpolated corrections (IC). In the IC method, a few high level MEP points (the three stationary points in our case) are calculated, but an affordable low-level reaction path is calculated as well. Next, the *differences* between the high level curve (which we want), and the low-level curve (which we have) are interpolated from the differences between the high level points and the corresponding points on the low-level curve. These interpolated differences are used as "corrections" to the entire low-level reaction path (hence the name interpolated corrections) yielding an approximate high-level reaction path.

We used the IC method as developed by Hu[20] et al. In particular we used the Eckart fit corresponding to two reactant species and two product species and no intermediate complexes. The exact correction function for the low-level curve is

$$\Delta V(s) = V_{\mathrm{MEP,HL}}(s) - V_{\mathrm{MEP,LL}}(s) \tag{1}$$

where s is the signed distance through mass-scaled coordinates along the MEP, $V_{\mathrm{MEP,HL}}(s)$ is the high-level curve we seek to approximate, and $V_{\mathrm{MEP,LL}}(s)$ is the low-level curve we have. $V_{\mathrm{MEP,HL}}(s)$ and $V_{\mathrm{MEP,LL}}(s)$ are Born−Oppenheimer, "classical" potential energies. Since we have $V_{\mathrm{MEP,LL}}(s)$, we know $\Delta V(s)$ at $s = \pm\infty$,0. The values of V and ΔV at $s = 0$ are called $V^{\neq}$ and $\Delta V^{\neq}$. When $\Delta V(s = 0) > \Delta V(s = \pm\infty)$ or $\Delta V(s = 0) < \Delta V(s = \pm\infty)$, the second inequality holding for the reaction under study, we assume that the maximum or minimum of the correction function appears at $s = 0$, and we *approximate* it as an Eckart function, which is given by

$$\Delta V(s) = \frac{AY}{1+Y} + \frac{BY}{(1+Y)^2} + C \tag{2}$$

$$Y = \exp\left(\frac{s - S_0}{L}\right) \tag{3}$$

where

$$A = \Delta V(s = +\infty) - \Delta V(s = -\infty) \tag{4}$$

$$C = \Delta V(s = -\infty) \tag{5}$$

$$B = (2\Delta V^{\neq} - A - 2C) \pm 2[(\Delta V^{\neq} - C)(\Delta V^{\neq} - A - 2C)]^{1/2} \tag{6}$$

$$S_0 = -L \ln\left(\frac{A+B}{B-A}\right) \tag{7}$$

In eq 6, the ± sign is positive if $\Delta V(s = 0) > \Delta V(s = \pm\infty)$ and negative if $\Delta V(s = 0) < \Delta V(s = \pm\infty)$. The range parameter L is obtained from the low-level fit and then used in the same equation for the high-level interpolation.

The determinant of the moment of inertia tensor $\mathbf{I}(s)$ for the generalized transition state also needs to be corrected. Since $\mathbf{I}(s)$ approaches infinity as s approaches positive infinity (reactants getting infinitely far apart) or negative infinity (products getting infinitely far apart), we cannot use the method presented above. Instead, we correct the low-level moment of inertia tensor $\mathbf{I}_{\mathrm{LL}}$ with a simple multiplicative factor a such that

$$|\mathbf{I}_{\mathrm{HL}}(s)| = \alpha|\mathbf{I}_{\mathrm{LL}}(s)| \tag{8}$$

where

$$\alpha = \frac{|I_{HL}(s = 0)|}{|I_{LL}(s = 0)|} \tag{9}$$

The results of the IC procedure are then used for variational transition-state calculations and zero and/or small curvature tunneling calculations.

The same Eckart function used for the potential correction function is also used for the frequency correction function if $\Delta\omega_m(s = 0) > \Delta\omega_m(s = \pm\infty)$ or $\Delta\omega_m(s = 0) < \Delta\omega_m(s = \pm\infty)$, where

$$\Delta\omega_m(s) = \Delta\omega_{m,HL}(s) - \omega_{m,LL}(s) \tag{10}$$

B. Electronic Structure. All ab initio electronic structure calculations were performed with the ACES II[21] and Gaussian 94[22] programs. These programs were chosen for the range of

calculations they can perform on open-shell systems. Especially important for reaction path following is the ability of ACES II to calculate analytic first and second derivatives.

The methods used were self-consistent field (SCF),[23] many-body perturbation theory (MBPT(2)),[24] and coupled-cluster singles-and-doubles (CCSD)[25] with a perturbative triples correction (CCSD(T)).[26,27] Unrestricted Hartree−Fock (UHF)[28] reference functions were used for open-shell and closed-shell species. Analytical gradients[29,30] were used for reaction path computation and all geometry optimizations. Where SCF or MBPT(2) was used, Hessians were calculated analytically.[31−34] As ACES II does not support analytic Hessians for CCSD(T) methods, CCSD(T) Hessians were calculated numerically by finite differences of gradients. Spin contamination was monitored by the correlated spin multiplicity[35] and found not to be significant. $S^2 = 2.09$ is typical for the triplet OOH−H transition state.

Five contracted Gaussian basis sets were used. The size and flexibility of each basis set was chosen such that a balance was obtained with respect to the level of treatment of correlation. Basis set 1, commonly known as Dunning's D95*, was the double-ζ plus polarization (DZP) type. The DZP basis for hydrogen was a 2s contraction[36] by Dunning, using a scale factor of 1.44, of a set of 4s primitives by Huzinaga.[37] This was augmented with a polarization p function primitive of exponent 1.0. The DZP basis for oxygen was a 4s2p contraction[36] by Dunning of a set of 9s5p primitives[37] by Huzinaga. This was augmented with a Cartesian, polarization d function primitive of exponent 0.85.[38] Basis set 2 was the triple-ζ valence plus polarization (TZVP) type. The TZVP set for Hydrogen was a 3s contraction[39] of a 6s primitive set.[37] This was augmented with a polarization p function primitive of exponent 0.75. The TZVP set for oxygen was a 5s3p contraction[39] of a set of 10s6p primitives.[37] This was augmented with a Cartesian, polarization d function primitive of exponent 0.85. In basis set 3, the hydrogen s set and the oxygen sp set were the same as those in basis set 2. The single oxygen, polarization d function in basis set 2 was substituted with 2d and 1f functions. The d exponents for oxygen were 2.314 and 0.645 and the f function exponent for oxygen was 1.428. Basis set 4 was the correlation-consistent quadruple-ζ valence plus polarization (PVQZ) basis set.[40,41] The PVQZ set for hydrogen was a 4s contraction of a 6s primitive set. This was augmented with 3p, 2d, and 1f functions. The oxygen PVQZ set was a 5s4p contraction of a 12s6p primitive set, with 3d, 2f, and 1g Cartesian polarization functions. Basis set 5 adds diffuse functions to basis set 4. Diffuse functions for hydrogen were 1s, and 1p, including 1d and 1f Cartesian functions. Diffuse functions for oxygen were 1s, and 1p, including 1d, 1f, and 1g Cartesian functions. Basis sets 1, 2, and 3 were used for the geometry optimizations and gradient and Hessian calculations. Basis sets 4 and 5 were used only for single point calculations.

The rate constant calculations were carried out using the direct dynamics program ACESRATE,[42] which is an integration of the VTST dynamics program POLYRATE[16] and the ACES II[21] electronic structure package.

III. Results and Discussion

A. Reaction Energetics. The calculation of an accurate rate constant requires a precise potential energy surface. The most important points on the PES are the stationary points: reactants, products, and the saddle point. To gauge the convergence of our PES, we performed geometry optimizations for each of the stationary points at a series of increasing basis sets and correlation treatments. The optimized geometries for reactants, products, and transition state for MBPT(2)/basis 1, MBPT(2)/basis 2, CCSD(T)/Basis 1, CCSD(T)/basis 2 and CCSD(T)/basis 3 are summarized in Table 1. The calculations suggest that we have converged the reactant HO bond length to within 0.011 Å and the OO bond length to 0.023 Å. The OOH bond angle is converged to 0.5°. In addition, the reactant bond lengths computed at the highest level, CCSD(T)/basis 3, agree with experiment to within 0.001 Å and the bond angles agree to within 1°. This is excellent convergence and suggests that the geometry of the reactants on the PES is very accurate. Our products are similarly converged with both bond lengths differing by less than 0.025 Å and differ from experiment by only 0.001 and 0.003 Å in the H_2 and O_2 bond lengths, respectively. The deviations between the CCSD(T)/basis 2 and CCSD(T)/basis 3 transition state geometry optimization are also small for the transition state bond lengths. The largest difference is just 0.022 Å. The bond angles appear to be converged to less than 1°. The CCSD(T)/basis 3 geometries give a fairly accurate description of the stationary point geometries on the PES.

TABLE 1: $H + HO_2 \rightarrow H_2 + O_2$ Optimized Geometries for the Reactants, Transition State, and Products[a]

species	R_{HH}	R_{HO}	R_{OO}	∠OOH	∠OHH
experiment					
reactants		0.971	1.331	104.3	
products	0.742		1.207		
MBPT(2)/basis 1					
reactants		0.976	1.329	104.4	
transition state	1.061	1.094	1.287	108.2	179.5
products	0.735		1.250		
MBPT(2)/basis 2					
reactants		0.980	1.330	104.2	
transition state	1.065	1.097	1.287	107.9	179.8
products	0.741		1.247		
CCSD(T)/basis 1					
reactants		0.976	1.352	104.0	
transition state	1.181	1.058	1.320	107.0	178.2
products	0.739		1.233		
CCSD(T)/basis 2					
reactants		0.982	1.355	103.7	
transition state	1.204	1.056	1.324	106.6	178.0
products	0.746		1.232		
CCSD(T)/basis 3					
reactants		0.971	1.332	104.2	
transition state	1.200	1.048	1.301	107.0	177.8
products	0.743		1.210		

[a] Bond lengths are given in angstroms and bond angles are in degrees. Experimental numbers are given for the reactants[43] and products.[44]

The energetics for reaction R6c computed over the range of correlation levels and basis sets discussed above are summarized in Table 2. For each of the three stationary points, reactants, products, and the transition state, the total electronic energy is given in hartrees. In determining the interaction energy, we define the zero of energy to be infinitely separated reactants at the bottom of the well. The electronic interaction energy, ΔV_{MEP}, is just the difference in electronic energies between the reactants and each of the other stationary points. This quantity is given in kcal/mol in the table. The third quantity given in the table, ΔV_a^G, is the ground-state vibrationally adiabatic energy. This is equal to ΔV_{MEP} plus the harmonic ground-state vibration zero point energy. It is also reported in kcal/mol. Note that the CCSD(T)/basis 4 single point results given in Table 2 are single point calculations using CCSD(T)/basis 3 geometries.

Table 2 shows the converging trend in barrier height and in exoergicity with increasing level of theory. CCSD(T)/basis 5 single point is the highest level calculation, giving a barrier

TABLE 2: Energetics for Reaction (R6c) for Reactants, Transition State, and Products[a]

	reactants		transition state			products		
calculation	total E	ΔV_a^G	total E	ΔV_{MEP}	ΔV_a^G	total E	ΔV_{MEP}	ΔV_a^G
MBPT(2)/Basis 1	−151.07146	9.19	−151.05950	7.50	15.58	−151.16937	−61.44	−52.81
MBPT(2)/Basis 2	−151.11586	8.88	−151.10520	6.69	14.70	−151.21135	−59.92	−51.55
CCSD(T)/Basis 1	−151.10244	8.96	−151.09568	4.24	11.82	−151.19187	−56.11	−47.40
CCSD(T)/Basis 2	−151.1422?	8.84	−151.14701	3.02	10.59	−151.23461	−54.97	−46.43
CCSD(T)/Basis 3	−151.25475	8.95	−151.25071	2.53	11.70	−151.34250	−55.06	−46.49
CCSD(T)/Basis 4	−151.33874		−151.33503	2.33		−151.42554	−54.47	
CCSD(T)/Basis 5	−151.34994		−151.34650	2.16		−151.43578	−53.86	

[a] The basis 4 and basis 5 single point energies are computed using the CCSD(T)/basis 3 optimized geometries. All other energies are calculated at geometries optimized at the same level of theory. The zero of energy is at infinitely separated reactants in their ground electronic state. Total Energies are given in Hartrees. ΔV_{MEP} and ΔV_a^G are given in kcal/mol.

TABLE 3: Vibrational Frequencies for the Reactants, Transition State, and Products for Reaction (R6c)[a]

		MBPT(2)		CCSD(T)		
molecule	expt	basis 1	basis 2	basis 1	basis 2	basis 3
OOH						
ν_1 (cm^{-1})		3741	3690	3717	3629	3675
ν_2 (cm^{-1})		1445	1328	1422	1410	1441
ν_3 (cm^{-1})		1242	1194	1128	1147	1144
[OOHH]$^{\neq}$						
ν_1 (cm^{-1})		1645	2691	1654	1709	1766
ν_2 (cm^{-1})		1424	1770	1398	1391	1699
ν_3 (cm^{-1})		1344	1394	1193	1163	1418
ν_4 (cm^{-1})		824	619	710	694	1193
ν_5 (cm^{-1})		411	534	347	341	336
ν_6 (cm^{-1})		2657i	1343i	2018i	1727i	1764i
H_2						
ν_1 (cm^{-1})	4395	4621	4462	4515	4431	4403
O_2						
ν_1 (cm^{-1})	1580	1415	1399	1580	1543	1594

[a] Results are for the three levels of geometry optimizations: MBPT(2)/basis 1, MBPT(2)/basis 2, CCSD(T)/basis 1, CCSD(T)/basis 2, and CCSD(T)/basis 3. Experimental frequencies are given for H_2,[43] O_2,[43] and OOH.

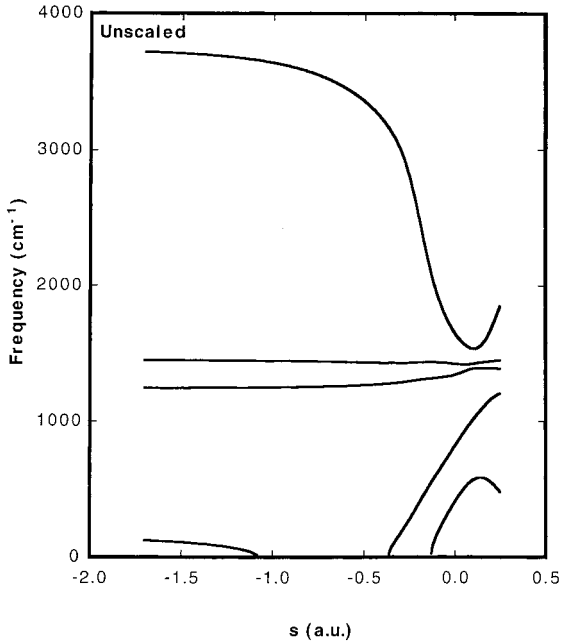

Figure 1. Frequencies along the reaction path for the unscaled MBPT(2)/basis 1 calculations.

height of 2.16 kcal/mol. This value represents a 0.17 kcal/mol decrease in barrier height when increasing the basis from 3d 2f 1g (basis 4, single point) to 3d 2f 1g plus 1s 1p 1d 1f 1g (basis 5, single point) on the heavy atoms. This relatively small change (7.3%) in barrier height, coupled with the excellent agreement of our results with experiment, indicates that the barrier is fairly well converged. Further testing for convergence of the barrier would require calculations at larger basis sets, but we have reached our computational limit for the present. Furthermore, the effect on our final results of the remaining uncertainty in the barrier height is small compared to the remaining uncertainty in the highest level zero-point energies, calculated at only CCSD(T)/basis 3. Thus, the energetics used for the high-level direct dynamics MEP scaling procedure were computed from the CCSD(T)/basis 5 single point energies for the CCSD(T)/basis 3 optimized geometries.

The low-level MEP was calculated at the MBPT(2)/basis 1 level. The cost of computing an MEP at a higher level correlation treatment is prohibitive. An MBPT(2) MEP calculation with a basis larger than basis 1, e.g., MBPT(2)/basis 2, would be more accurate than MBPT(2)/basis 1, but the extra cost is not worth the gain in accuracy as the differences in barrier height and exoergicity between these two methods is small compared to the energy difference between either method and the high-level energetics to which the low-level MEP is scaled.

B. Dynamics. The rate constants were computed using CVT. The tunneling correction, κ, was computed using the centrifugal-dominant small-curvature semiclassical adiabatic ground state (CD-SCSAG)[16] method. The coordinates were all scaled to a reduced mass m of 0.94737 amu. The MEP was computed using the method of steepest descents in the range $-1.7 \le s \le 0.25a_0$ with a step size between gradient calculations equal to $\delta s = 0.001a_0$ and a distance between Hessian calculations equal to $\Delta s = 0.005a_0$. These step sizes represent convergence of the rate constants to at least three significant digits. All vibrational degrees of freedom were treated using the harmonic approximation.

The room-temperature rate constant (300 K) calculated for the MBPT(2)/basis 1 (low-level) MEP was 5.82×10^{-14} cm^3 molecule^{-1} s^{-1}. This result is for CVT with CD-SCSAG (small curvature) tunneling corrections.

Because of the high barrier at this level of theory, the CVT/CD-SCSAG calculation seriously underestimates the rate constant (see final results in Table 8 for comparison). The error resulting from the inaccurate MBPT(2)/basis 1 energetics was corrected using the method of interpolated corrections (IC) discussed earlier.

MBPT(2)/basis 1 results were used as the low level and CCSD(T)/basis 3 single point results were used as the high level. The range parameter $L = 0.32$ was obtained by the Eckart function fitting procedure discussed in Hu et al. using the MBPT(2)/basis 1 results. The moment of inertia along the reaction path was scaled by the method given in Hu et al., using the ratio of the high- and low-level saddle point moments of inertia computed from the geometries given in Table 1. In

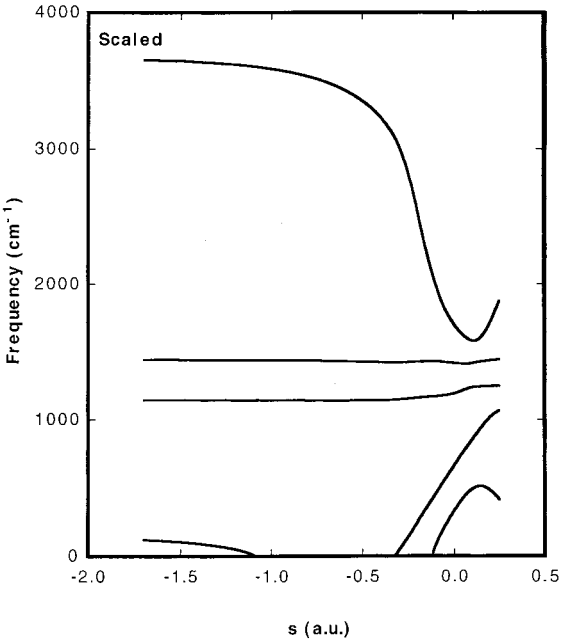

Figure 2. Frequencies along the reaction path for the scaled MBPT(2)/basis1//CCSD(T)/basis 3 calculations.

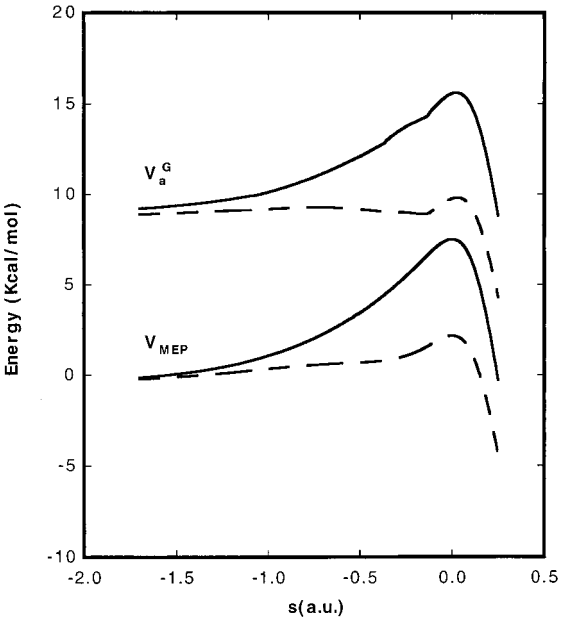

Figure 3. Minimum energy path (V_{MEP}) and adiabatic potential energy curve (V_a^G) for the unscaled (solid lines) MBPT(2)/basis 1, and scaled (dashed lines) MBPT(2)/basis1//CCSD(T)/basis 3 calculations.

addition, frequencies were also scaled as described in Hu et al. Frequencies for all optimized species are summarized in Table 3. The frequencies along the low-level, unscaled reaction path are shown in Figure 1. Figure 2 shows the frequencies along the new, scaled (by IC) reaction path. Using the scaled frequencies along the MEP, a new, adiabatic potential energy curve was computed. Figure 3 shows the unscaled (solid curves) and scaled (dashed curves) V_{MEP} and V_a^G.

The scaled quantities were then used to compute, over a wide range of temperatures, the CVT/CD-SCSAG rate constants presented in Table 4. Included in Table 4 are experimental results by Hack et al.,[7] Keyser,[11] and Sridharan et al.[10] Table 4 shows excellent (within a few percent) agreement between the theoretical rate constants and the best, most recent, most consistent experimental values: those by Keyser[11] and Sridharan.[10] The theoretical rate constants over the temperature range 150−800 K are not Arrhenius, as is evident from the Arrhenius plot shown in Figure 4.

TABLE 4: Forward CVT/CD-SCSAG Rate Constants for OOH + H→ O_2 + H_2[a]

temp	CVT/SCT	Keyser	Δ%	Sridharan	Δ%
150	5.81×10^{-12}				
190	6.00×10^{-12}				
200	6.06×10^{-12}				
250	6.41×10^{-12}	6.96×10^{-12}	−7.9%		
295	6.80×10^{-12}	6.96×10^{-12}	−2.3%		
296	6.81×10^{-12}	6.96×10^{-12}	−2.2%	6.7×10^{-12}	1.6%
300	6.85×10^{-12}	6.96×10^{-12}	−1.6%		
308	6.93×10^{-12}				
400	7.90×10^{-12}				
600	1.05×10^{-11}				
800	1.37×10^{-11}				

[a] Results are for the MBPT(2)/basis 1 low-level path scaled by IC to CCSD(T)/basis 5 single point energetics. Experimental values are included for comparison. Rate constants are given in cm^3 $molecule^{-1}$ s^{-1}. Temperature is given in K.

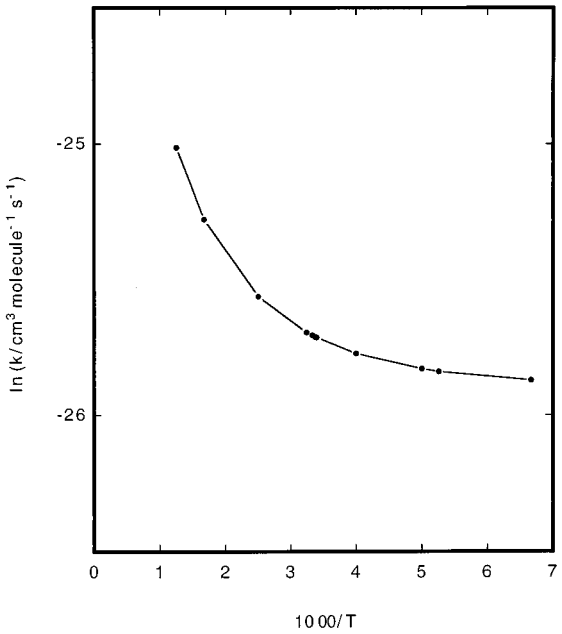

Figure 4. Arrhenius plot of the final CVT rate constants.

IV. Conclusion

Rate constants for the reaction OOH + H → H_2 + O_2 have been calculated, and are in excellent agreement with experiment at room temperature. No experimental values for low temperatures are available for comparison, but given the impressive agreement with experiment at room temperature, our calculated low temperature values should shed much needed light on the low temperature behavior of this reaction rate constant, critical to the concentration of ozone at the extremely cold mesopause. Direct dynamics has performed well, yielding room-temperature rate constants that agree with experiment to within a few percent.

Acknowledgment. The authors thank Peter Taylor for many helpful discussions. This work was supported by the National Science Foundation. Some computer resources were provided by a grant from the San Diego Supercomputer Center.

References and Notes

(1) Clyne, M. A. A.; Thrush, B. A. *Proc. R. Soc. London, Ser. A* **1963**, *275*, 559.

(2) Dodonov, A. F.; Lavroskaya, G. K.; Talroze, V. L. *Kinet. Katal.* **1969**, *10*, 573.

(3) Bennet, J. E.; Blackmore, D. R. *Proceedings of the 13th International Symposium on Combustion*, 1971, p 57.

(4) Westenberg, A. A.; De Haas, N. *J. Phys. Chem.* **1972**, *76*, 1586.

(5) Day, M. J.; Thompson, K.; Dixon-Lewis, G. *Proceedings of the 14th International Symposium on Combustion*, 1973, p 47.

(6) Baldwin, R. R.; Fuller, M. E.; Hillman, J. S.; Jackson, D.; Walker, R. W. *J. Chem. Soc., Faraday Trans. 1* **1974**, *70*, 635.

(7) Hack, W.; Wagner, H. G.; Hoyermann, K. *Ber. Bunsen-Ges. Phys. Chem.* **1978**, *82*, 713.

(8) Hack, W.; Preuss, A. W.; Wagner, H. G.; Hoyermann, K. *Ber. Bunsen-Ges. Phys. Chem.* **1979**, *83*, 212.

(9) Thrush, B. A.; Wilkinson, J. P. T. *Chem. Phys. Lett.* **1981**, *84*, 17.

(10) Sridharan, U. C.; Qiu, L. X.; Kaufman, F. *J. Phys. Chem.* **1982**, *86*, 4569.

(11) Keyser, L. F. *J. Phys. Chem.* **1986**, *90*, 2994.

(12) Truhlar, D. G.; Garrett, B. C. *Annu. Rev. Phys. Chem.* **1984**, *27*, 1.

(13) Truhlar, D. G.; Isaacson, A. D.; Garrett, B. C. Generalize Transition State Theory. In *Theory of Chemical Reaction Dynamics*; Baer, M., Ed.; CRC Press: Boca Raton, 1985; Vol. 4; p 1.

(14) Truhlar, D. G.; Brown, F. B.; Steckler, R.; Isaacson, A. D. The Representation and Use of Potential Energy Surfaces in the Wide Vicinty of a Reaction Path for Dynamics Calculations on Polyatomic Reactions. In *The Theory of Chemical Reaction Dynamics*; Clary, D. C., Ed.; D. Reidel: Dordrecht, Holland, 1986; pp 285−329.

(15) Truhlar, D. G.; Garrett, B. C. *J. Chim. Phys. Phys.*−*Chim. Biol.* **1987**, *84*, 365.

(16) Steckler, R.; Hu, W.-P.; Liu, Y.-P.; Lynch, G. C.; Garrett, B. C.; Isaacson, A. D.; Melissas, V. S.; Lu, D.-h.; Troung, T. N.; Rai, S. N.; Hancock, G. C.; Lauderdale, J. G.; Joseph, T.; Truhlar, D. G. *Comput. Phys. Commun.* **1995**, *88*, 341−343.

(17) Page, M. *Comput. Phys. Commun.* **1994**, *84*, 115−130.

(18) Truhlar, D. G. Direct Dynamics Method for the Calculation of Reaction Rates. In *The Reaction Path in Chemistry: Current Approaches and Perspectives*; Heidrich, D., Ed.; Kluwer Academic Publishers: Dordrecht, Netherlands, 1995; pp 229−255.

(19) Peslherbe, G. H.; Hase, W. L. *J. Chem. Phys.* **1996**, *104*, 7882−7894.

(20) Hu, W.-P.; Liu, Y.-P.; Truhlar, D. G. *J. Chem. Soc. Faraday Trans. I* **1994**, *90*, 1715−1725.

(21) Stanton, J. F.; Gauss, J.; Watts, J. D.; Nooijen, M.; Oliphant, N.; Perera, S. A.; Szalay, P. G.; Lauderdale, W. J.; Gwaltney, S. R.; Beck, S.; Balková, A.; Bernholdt, D. E.; Baeck, K.-K.; Sekino, H.; Bartlett, R. J. ACES II; Quantum Theory Project, University of Florida: Gainesville, FL, 1994.

(22) Frisch, M. J.; Trucks, G. W.; Schlegel, H. B.; Gill, P. M. W.; Johnson, B. G.; Robb, M. A.; Cheeseman, J. R.; Keith, T. A.; Petersson, G. A.; Montgomery, J. A.; Raghavachari, K.; Al-Laham, M. A.; Zakerzewski, V. G.; Ortiz, J. V.; Foresman, J. B.; Cioslowski, J.; Stefanov, B. B.; Nanayakkara, A.; Challacombe, M.; Peng, C. Y.; Ayala, P. Y.; Chen, W.; Wong, M. W.; Andres, J. L.; Replogle, E. S.; Gomperts, R.; Martin, R. L.; Fox, D. J.; Binkley, J. S.; Defrees, D. J.; Baker, J.; Stewart, J. P.; Head-Gordon, M.; Gonzalez, C.; Pople, J. A. GAUSSIAN 94 Gaussian, Inc.: Pittsburgh, PA, 1995.

(23) Pople, J. A.. In *Applications of Electronic Structure Theory*; Schaefer, H. F., III, Ed.; Plenum Press: New York, 1977.

(24) Moller, C.; Plesset, M. S. *Phys. Rev.* **1934**, *46*, 618.

(25) Purvis III, G. D.; Bartlett, R. J. *J. Chem. Phys.* **1982**, *76*, 1910−1918.

(26) Urban, M.; Noga, J.; Cole, S. J.; Bartlett, R. J. *J. Chem. Phys.* **1985**, *83*, 4041−4046.

(27) Raghavachari, K.; Trucks, G. W.; Pople, J. A.; Head-Gordon, M. *Chem. Phys. Lett.* **1989**, *157*, 479−483.

(28) Pople, J. A.; Nesbet, R. K. *J. Chem. Phys.* **1954**, *22*, 571.

(29) Gauss, J.; Stanton, J. F.; Bartlett, R. J. *J. Chem. Phys.* **1991**, *95*, 2623−2638.

(30) Watts, J. D.; Gauss, J.; Bartlett, R. J. *Chem. Phys. Lett.* **1992**, *200*, 1.

(31) Pople, J. A.; Krishnan, R.; Schlegel, H. B.; Binkley, J. S. *Int. J. Quantum Chem. Symp.* **1979**, *13*, 225−241.

(32) Handy, N. C.; Amos, R. C.; Gaw, J. F.; Rice, J. E.; Simandiras, E. D. *Chem. Phys. Lett.* **1985**, *120*, 151−158.

(33) Harrison, R. J.; Fitzgerald, G. B.; Laidig, W. D.; Bartlett, R. J. *Chem. Phys. Lett.* **1986**, *124*, 291−294.

(34) Stanton, J. F.; Gauss, J.; Bartlett, R. J. *Chem. Phys. Lett.* **1992**, *195*, 194−199.

(35) Purvis III, G. D.; Sekino, H.; Bartlett, R. J. *Collect. Czech. Chem. Commun.* **1988**, *53*, 2203.

(36) Dunning, T. H., Jr. *J. Chem. Phys.* **1970**, *53*, 2823−33.

(37) Huzinaga, S. *J. Chem. Phys.* **1965**, *42*, 1293.

(38) Dunning, T. H., Jr.; Hay, P. J. In *Methods of Electronic Structure Theory*; Schaefer, H. F., III, Ed.; Plenum: New York, 1977.

(39) Dunning, T. H., Jr. *J. Chem. Phys.* **1971**, *55*, 716.

(40) Woon, D. E.; Dunning, T. H., Jr. *J. Chem. Phys.* **1993**, *98*, 1358.

(41) Dunning, T. H., Jr. *J. Chem. Phys.* **1989**, *90*, 1007.

(42) Steckler, R.; Thurman, G. M. *J. Chem. Phys.* **1997**, *106*, 3926−3933.

(43) Herzberg, G. F. R. S. *Molecular Spectra and Molecular Structure*, Second reprint edition ed.; Robert E. Krieger Publishing Company: Malabar, Florida, 1989; Vol. I. Spectra of Diatomic Molecules.

(44) Lubic, K. G.; Amano, T.; Uehara, H.; Kawaguchi, K.; Hirota, E. *J. Chem. Phys.* **1984**, *81*, 4826−4831.